Indian Journal of Biochemistry & Biophysics
Vol. 63, March 2026, pp. 253-266
DOI: 10.56042/ijbb.v63i3.18045

DFT-Based Analysis of 2, 3-dimethyl-2-(3-oxobutyl)-cyclohexanone: Structural, Electronic, Vibrational, and Molecular docking studies for potential anti-cancer applications

Revathi G[1], Rajesh P[2]*, Dhanalakshmi E[3], Kayashrini S[4], Lawrence M[5], Prabhaharan M[6] & Arularasan P[7]

[1, 2 & 4]Department of Physics, School of Basic Sciences, Vels Institute of Science, Technology & Advanced Studies, Pallavaram, Chennai-600 117, Tamil Nadu, India

[3]Department of Physics, Vel Tech Multi Tech Dr. Rangarajan Dr. Sakunthala Engineering College, Avadi, Chennai-600 062, Tamil Nadu, India

[5]Department of Physics, Loyola Institute of Technology, Palanchur, Chennai-600 123, Tamil Nadu, India

[6]Department of Physics, Saveetha School of Engineering, Saveetha Institute of Medical and Technical Sciences (SIMATS), Chennai-602 105, Tamil Nadu, India

[7]Post Graduate Department of Physics, Dwaraka Doss Goverdhan Doss Vaishnav College, Chennai-600 106, Tamil Nadu, India

Received 19 March 2025; *revised 24 April 2025*

The antimicrobial, antibacterial, antioxidant, anti-inflammatory, and anticancer activities of C2D3O (2, 3-dimethyl-2-(3-oxobutyl)-cyclohexanone) are demonstrated. Through the use of FT-IR, UV-Vis, and DFT methodologies, this study investigates its medical applications. The B3LYP/6-311++G(d, p) approach was used to examine the molecular electrostatic potential (MEP), HOMO-LUMO, and geometrical characteristics. High stabilization interactions, including hydrogen bonding and charge delocalization, were computed in 3TMH molecules using the NBO 3.1 tool. Both single and double-bond stability was demonstrated by the optimized structure, which was in good agreement with XRD results.A strong correlation was found between theoretical and experimental vibrational frequencies, with electronic transitions (n→π, n→σ transitions**) identified via TD-DFT. The Veda 04 software confirmed an excellent match between observed and predicted FT-IR spectra. Chemical interactions were examined through ELF-LOL projection mapping, while RDG analysis (using Multiwfn 3.4.1) highlighted strong attraction, repulsion, and weak interactions. Finally, molecular docking of C2D3O with 8D59 demonstrated a binding energy of -4.94 kcal/mol, suggesting potential biomedical applications.

Keywords: 8D59, Drug-likeness, FT-IR, Topological properties, UV–visible

Colon cancer is the second leading cause of cancer-related death worldwide. Colorectal cancer is one type of cancer that affects the rectum or colon (large intestine). It is one of the most common types of cancer worldwide. It may cause fatalities or severe injuries. Many people will show no symptoms in the early stages of the illness. Over 1.9 million new cases of colorectal cancer and over 930, 000 deaths from the disease were predicted to occur worldwide in 2020. Mortality and incidence rates showed notable regional variations[1]. According to the literature review, the cyclohexanone 2, 3-dimethyl-2-(3-oxobutyl)-correlated has anti-cancer properties[2]. The extra descriptors imply certain groups connected to the cyclohexanone ring, which is a six-membered cyclic ketone. One ketone functional group is present in the six-membered ring of cyclohexanone, and the second and third carbon atoms of the ring are joined by 2, 3-dimethyl CH_3 a 3-oxobutyl group joined to the cyclohexanone ring's second carbon. A ketone (oxo) group is present on the third carbon of the four-carbon chain that makes up the 3-oxobutyl group. The carbons in the cyclohexanone ring are represented by the letters C_1 to C_6. Methyl groups (CH_3) are joined to C_2 and C_3, while the $_2$-CO-CH_3 chain (3-oxobutyl) is joined to C_2. The way the groups are joined to the cyclohexanone ring is shown graphically by this structure. Its molecular weight is 196.29 g/mol, and its molecular formula is C12H20O2.Because of their capacity to interact with biological molecules and processes implicated in the growth of cancer cells, cyclohexanone derivatives have been investigated for their possible anticancer effect. Ways such as inducing apoptosis, inhibiting cell growth, having anti-angiogenic qualities, and preventing metastases. Because cyclohexanone and its derivatives can disrupt the development and survival of cancer cells, they have potential use in anticancer

*Correspondence:
E-mail: rajesh.ncc5coy@gmail.com

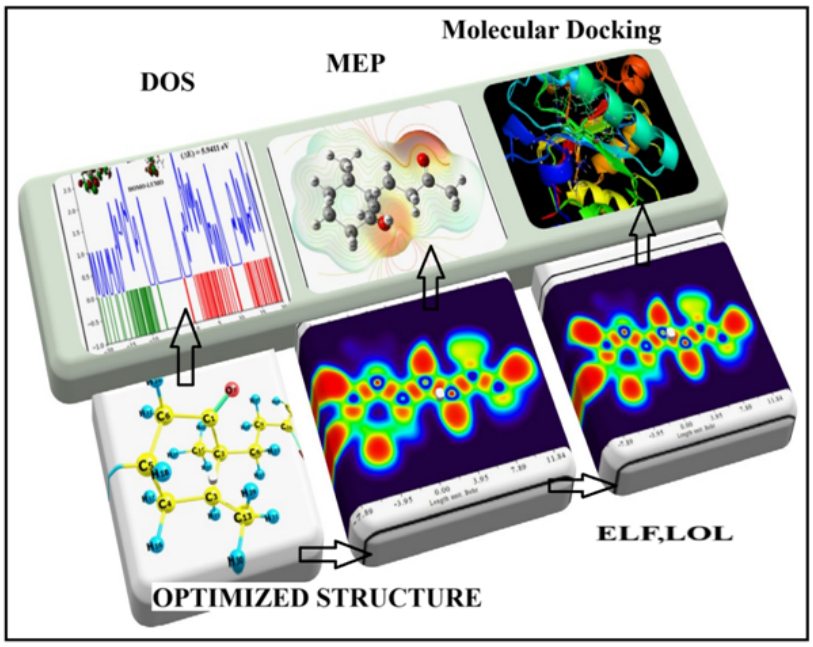

Graphical abstract

treatment. Although there may not be much precise data on the 2-(3-oxobutyl) group's anticancer action on its own, the fact that it is present in several bioactive compounds points to promise. New anticancer medications can be developed with the help of ongoing research into related substances and their processes[3]. To the best of our knowledge, the density functional computation (DFT) has not yet been performed, according to the study work mentioned above. By using the Soxhlet procedure, which falls under the Gas Chromatography-Mass Spectrometry (GC-MS) technology, the C2D3O compound was extracted from *Hybanthus enneaspermus* crude. The C2D3O compound was then reported for its structure and conformation. Infrared data on C2D3O molecules was connected with the optimized structural attributes, simulated FT-IR, and UV-vis spectra produced by the B3LYP/6-311++G (d.p) procedure. DFT was used to assess the reported biological activity from the NBO study, MEP surface, Fukui function, PES scan, and energy gap. Physical-chemical properties that demonstrated favorable aspects of drug-likeness were also estimated using the topological parameter, RDG analysis, and Lipinski's criteria. Good ligand-protein interaction on C2D3O molecules against anti-cancer activity was found by the docking studies.

Experimental techniques detail

The Shimadzu QP2010 Plus gas chromatography-mass spectrometry (GC-MS) method was used to evaluate the crude material. With an injection temperature of 250°C, a non-polar MS capillary column covered with polydimethylsiloxane (30 m in length, 0.25 mm inner diameter, and 0.25 µm film thickness) was employed. A retention duration of 25 minutes was shown by the GC-MS spectra[4]. A lot of bio-compounds were detected in the GC-MS data; however, because of its possible anti-cancer effects, one measurable phytochemical compound, C2D3O, was chosen for more study. Sigma-Aldrich provided a 99% pure C2D3O sample for examination. Fourier-transform infrared (FT-IR) spectroscopy was used to investigate the C2D3O sample in the 4000–400 cm^{-1} region. At room temperature, measurements were made using a Perkin Elmer FT-IR spectrophotometer that used the KBr pellet technique with a spectral resolution of 4.0 cm^{-1}. Furthermore, a Shimadzu UV-3600+ equipment was used for ultraviolet-visible (UV-Vis) spectroscopy, recording wavelengths between 300 and 100 nm. For the analysis, a quartz cell measuring 1 cm in diameter and 0.5 nm in slit width was used[5]. At SRM College of Science in Kattankulathur, Chengalpattu district, Tamil Nadu, India, the GC-MS, FT-IR, and UV-Vis spectral analyses were carried out.

Computational details

In this study, the molecular structure of C2D3O was analyzed using the B3LYP/6-311++G(d, p) method within the DFT framework[6]. For geometry

visualization, HOMO-LUMO analysis, PES scan, and MEP charting, GaussView 5.0 and ChemCraft 1.8 were utilized[7]. MEP, Fukui function, and NPA charges were among the structural and electronic characteristics that were investigated. Vibrational analysis was conducted using Veda 04, with PED% interpretation and frequency scaling. The HOMO-LUMO gap and reactivity indices were ascertained by molecular orbital analysis, whereas TD-DFT was utilized for UV-Vis spectra in the gas and solvent phases. Intermolecular and intramolecular interactions were examined using NBO 3.1 software[8]. MULTIWFN 3.7 was used to calculate topological parameters (RDG, ELF, LOL), and Auto Dock 1.5.6 was used to conduct molecular docking studies for ligand-protein binding energy[9, 10].

Results and Discussion

GC–MS analyse

Mass spectrometry and chromatography are excellent tools for quantitative and qualitative analysis and for efficiently separating multicomponent mixtures at low concentrations. Purified bio-compounds (fatty acids, lipids) from medicinal plants, forensic investigations, and pollution studies are just a few of the many fields used for the GC-MS. A bio-component identified by mass spectrometry, C2D3O, was reported by the GC-MS analysis of the carbinol extract of the *H. Enneaspermus* plant in the current investigation. The results were compared and matched with data from the National Institute of Standards and Technology (NIST) data library and the PubChem databases[11]. Because of the chemical C2D3O's anticancer properties. Based on FT-IR, UV-Vis, and DFT spectral analysis. According to Figure 1, the CMIO chemical structure matched the molecular formula C12H20O2, molecular weight 196.14 g/mol, and retention time 21.48 min.

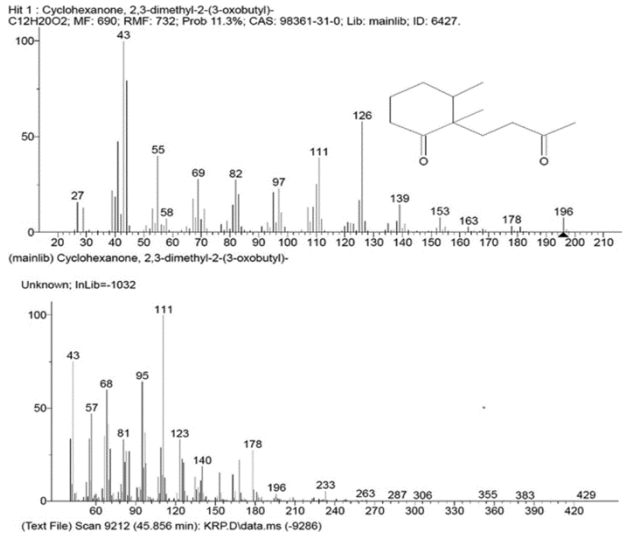

Fig. 1 — GC-MS analysis of C2D3O

Molecular geometry

In both biological and inorganic crystal formations, the ground-state geometrical parameters, such as bond lengths and angles are essential.

To investigate the optimal molecular shape and electrical characteristics of C2D3O, the DFT method more especially, the B3LYP/6-311++G(d, p) approach was used to identify its optimized geometry[12]. The ChemDraw program[13] was used to illustrate the molecular structure of C2D3O, and Figure 2 shows a scaled ball-and-stick model that represents its ideal shape. The molecule has a trigonal planar long-chain structure made up of one O-H bond, one C_3=C_2 link, five methyl (CH3) groups, one C-O bond, 19 C-C bonds, 39 C-H bonds, and one hydroxymethyl (CH2OH) group[14]. These bond parameters offer important information on how strong and stable the molecular interactions are inside the chemical complex[15]. Table 1 displays the findings of comparing the computed parameters of C2D3O with the values reported in the literature using XRD data.

A total of 60 bond lengths were discovered. Between C_{21} and H_{59}, the shortest bond length, 1.0914 (Å), is seen. C_7–C_8 show the greatest bond length of 1.5514 (Å). This title compound contains 115 bond angles. C_1-C_2-C_3 is linked to the largest bond angle of 128.322 (Å), whereas H_{39}-C_{12}-H_{40} has the lowest bond angle of 105.45 (Å). For the C-C and C-H bonds, the corresponding bond lengths range from 1.3407 Å to 1.551 Å, 1.091 Å to 1.103 Å, and 1.432 Å. The following bond lengths appear to match with XRD experimental values: C_1-O_{17} (1.432/1.425), C_3-C_4

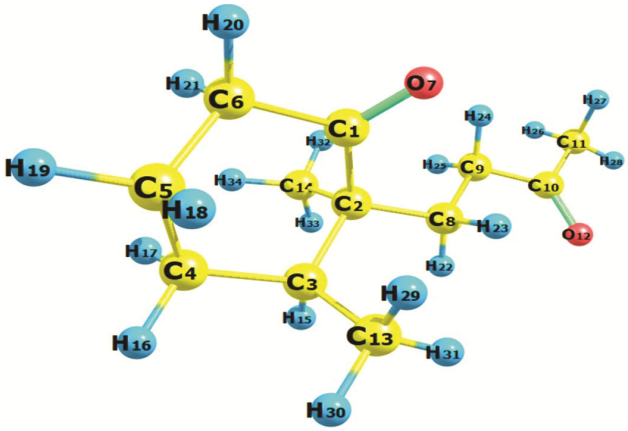

Fig. 2 — Optimized structure of C2D3O

(1.518/1.516), C_4-C_5 (1.531/1.523), C_5-C_6 (1.534/1.526), C_{11}-C_{19} (1.538/1.527), C_{12}-H_{39} (1.099/0.990), C_{12}-H_{40} (1.098/0.990), C_9-H_{34} (1.099/0.990), and C_9-H_{35} (1.094/0.990)[16-18]. The chemically determined bond angle values that match with the calculated XRD experimental bond angle are C_2-C_1-O_{17} (107.684 / 106.05), C_2-C_1-H_{23} (109.426 / 109.1), O17-C1-H23 (109.924 / 109.3), C10-C11-C19 (109.3049 / 109.17), and H50-C18-H51 (107.842 / 107.9)[19]. The number of shared electron pairs in C2D3O enhanced the molecular system's bond strength as well as the stability and strength of the attraction between C_3=C_2 (C_3=C_2>C_4-C_5). The acetyl group is denoted by CH3CO.

Mulliken atomic charge distribution

The distribution of atomic charges in molecular wave functions can be explained via the development of Mulliken charges investigations. The net atomic population is intimately related to the molecule's vibrational characteristics and the electronic structural changes brought on by atomic displacement. Its popular charge-splitting scheme effectively illustrates this link. The natural charge affects several characteristics of the molecular system, such as electronic structure, polarizability, and dipole moment. Title molecules C2D3O were obtained in the current investigation employing the B3LYP-D/6-311++G (d, p) level of theory, as shown in (Table 2).

Table 1 — Bond length, Bond angle

Bond length (Å)	B3LYP /6-311++G (d.p)	Experimental Data	Bond length (Å)	B3LYP /6-311++G (d.p)	Experimental Data
C1-C2	1.542	1.538	C8-C9	1.531	1.532
C1-C6	1.524	1.529	C8-H22	1.096	1.070
C1-O7	1.219	1.214	C8-H23	1.091	-
C2-C3	1.577	1.566	C9-C10	1.523	1.519
C2-C8	1.547	1.532	C9-H24	1.095	-
C2-C14	1.551	1.562	C9-H25	1.099	-
C3-C4	1.546	1.550	C10-C11	1.520	1.528
C3-C13	1.541	1.532	C10-O12	1.217	1.217
C3-H15	1.099	1.070	C11-H26	1.095	-
C4-C5	1.534	1.527	C11-H27	1.096	1.090
C4-H16	1.096	1.090	C11-H28	1.090	-
C4-H17	1.096	1.090	C13-H29	1.095	-
C5-C6	1.541	1.537	C13-H30	1.095	-
C5-H18	1.096	1.060	C13-H31	1.091	1.090
C5-H19	1.095	1.060	C14-H32	1.093	1.090
C6-H20	1.093	-	C14-H33	1.095	1.090
C6-H21	1.098	1.070	C14- H34	1.091	1.090
C2-C1-O6	116.7	117.5	C2-C8-C9	116.6	117.6
C2-C1-O7	122.4	122.6	C2-C8-H22	108.4	109
C6-C1-O7	120.8	121.6	C2-C8-H23	109.2	109.1
C1-C2-C3	107.9	-	C9-C8-H22	108.5	109.2
C1-C2-C8	110.8	110.4	C9-C8-H23	107.2	-
C1-C2-C14	108.8	108.8	H22-C8-H23	106.1	107.8
C3-C2-C8	110.0	110.5	C8-C9-C10	112.7	-
C3-C2-C14	109.2	-	C8-C9-H24	110.5	109.4
C8-C2-C14	109.8	109.8	C8-C9-H25	112.1	109.2
C2-C3-C4	111.9	111.5	C10-C9-H24	108.5	108.8
C2-C3-C13	113.1	112.4	C10-C9-H25	106.5	-
C2-C3-H15	106.0	-	H24-C9-H25	105.9	107.9
C4-C3-C13	110.4	-	C9-C10-C11	116.2	116.4
C4-C3-H15	107.6	108.8	C9-C10-O12	122.2	121.7
C13-C4-H15	107.2	107.7	C11-C10-O12	121.4	120.8
C3-C4-C5	112.6	113.4	C10-C11-H26	111.2	-
C3-C4-H16	108.7	108.9	C10-C11-H27	109.6	109.3
C3-C4-H17	110.2	110.8	C10-C11-H28	109.8	109.6
C5-C4-H16	109.8	-	H26-C11-H27	106.8	107.9
C5-C4-H17	109.1	-	H26-C11-H28	110.0	109.5
H_{16}-C_4-H_{17}	105.8	-	H27-C11-H28	109.2	109.5

(*Contd.*)

Table 1 — Bond length, Bond angle (*Contd.*)

Bond length (Å)	B3LYP /6-311++G (d.p)	Experimental Data	Bond length (Å)	B3LYP /6-311++G (d.p)	Experimental Data
C_4-C_5-C6	111.1	111	C3-C13-H29	112.3	-
C_4-C_5-H_{18}	110.0	-	C3-C13-H30	109.9	109.4
C_4-C_5-H19	110.4	-	C3-C13-H31	111.9	-
C_6-C_5-H18	109.0	109.1	H29-C13-H30	107.5	109.5
C_6-C_5-H_{19}	109.7	109.6	H29-C13-H31	107.3	109.5
H_{18}-C_5-H_{19}	106.2	-	H_{30}-C_{13}-H_{31}	107.4	109.5
C_1-C_6-C_5	111.5	-	C_2-C_{14}-H_{32}	111.6	110.3
C_1-C_6-H_{20}	107.7	-	C_2-C_{14}-H_{33}	109.5	109.5
C_1-C_6-H_{21}	108.5	-	C_2-C_{14}-H_{34}	112.9	-
C_5-C_6-H_{20}	112.0	114.5	H_{33}-C_{14}-H_{33}	107.7	107.3
C_5-C_6-H_{21}	109.1	109.5	H_{32}-C_{14}-H_{34}	107.2	107.9
H_{20}-C_6-H_{21}	107.6	107.7	H_{33}-C_{14}-H_{34}	107.5	107.8

A comprehensible qualitative image of chemists may be obtained from the natural Mullikan atomic charge distribution[20].While atoms C2, C3, C4, C5, C6, C7, C8, C9, C11, C12, C13, and C14 have nucleophilic charges and act as electron donors, atoms C1 and C10 have electrophilic charges and act as electron acceptors. Hydrogen has the largest positive charge among the hydrogen atoms (H15–H34)[21]. H23, which has the largest positive charge (0.149 a.u.), is the main site for nucleophilic attack, whereas the O7 and O12 sites are most vulnerable to electrophilic attack. Strong intermolecular bonding interactions are indicated by the O7 and O12 sites having the most negative charge (-0.447 a.u.)[22]. Both the cyclohexanone and the butyl group are attached to the second carbon atom of the cyclohexanone, which is symbolized by a double bond in oxygen, including ketone groups.C1 has a higher positive charge (0.423 a.u.) than the other carbon atoms, whereas C11 and C13 are associated with electro-negative charges (-0.379, -0.339)[23].

Table 2 — Mulliken atomic charge distribution

Atoms	Charges (a.u)	Atoms	Charges (a.u)
C_1	0.423	H_{18}	0.107
C_2	-0.007	H_{19}	0.100
C_3	-0.053	H_{20}	0.114
C_4	-0.191	H_{21}	0.116
C_5	-0.187	H_{22}	0.112
C_6	-0.243	H_{23}	0.149
O_7	-0.447	H_{24}	0.138
C_8	-0.171	H_{25}	0.130
C_9	-0.322	H_{26}	0.099
C_{10}	0.418	H_{27}	0.144
C_{11}	-0.379	H_{28}	0.141
O_{12}	-0.432	H_{29}	0.130
C_{13}	-0.339	H_{30}	0.097
C_{14}	-0.332	H_{31}	0.106
H_{15}	0.083	H_{32}	0.111
H_{16}	0.094	H_{33}	0.102
H_{17}	0.087	H_{34}	0.097

HOMO-LUMO

A molecule's HOMO and LUMO orbitals are essential for assessing its chemical stability, reactivity, softness, and hardness[24]. The most interactive orbital pair in a molecule is the HOMO, which donates electrons, and the LUMO, which accepts them. ELUMO indicates the molecule's ability to take electrons, while EHOMO indicates its ability to donate electrons. The investigated molecule has HOMO and LUMO energy values of -0.4465 eV and -6.3876 eV, respectively. These energy values aid in the explanation of hyper-polarizability and intramolecular charge transfer. 5.9411 eV is the determined value of the HOMO-LUMO energy gap (ΔE), a crucial measure of chemical reactivity. Higher kinetic stability and decreased reactivity are indicated by a bigger ΔE. The B3LYP/6-31+G(d) level of theory was used to investigate the frontier molecular orbitals (FMOs) of ADMA; (Fig. 3 & Table 3) show the relevant energy levels.

A theoretical method for forecasting the energy differential between the highest occupied and lowest empty molecular orbitals is the HOMO-LUMO computation[25, 26]. Based on its HOMO-LUMO energy values, Table 3 demonstrates the compound's strong electro negativity and electrophilic character. In industries including organic electronics, photovoltaics, telecommunications, imaging, and optical data processing, these electrical characteristics are crucial. According to the theoretical interpretation of the Mayr equation using the FMO and Eyring equations, a molecule's electrophilicity is defined by its LUMO energy, whereas its nucleophilicity is determined by its HOMO energy[27]. The investigated chemical shows improved stability because of its high ΔE value, which makes it a good option for optical applications like solar cells.

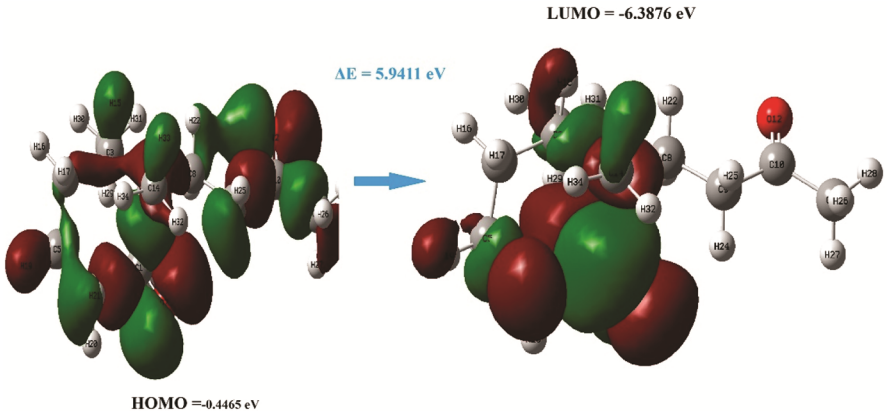

Fig. 3 — HOMO-LUMO parameters of C2D3O

Table 3 — HOMO-LUMO parameters of C2D3O

Parameters	Values	Parameters	Values
E_{HOMO} (eV)	-0.4465 eV	Chemical Potential (μ)	-3.0700 eV
E_{LUMO} (eV)	-6.3876 eV	Global electrophilicity (ω)	1.4537 eV
Energy Gap (ΔE)	5.9411 eV	Electron Acceptor Power (ώ+)	0.6281 eV
Ionization Potential (IP)	6.3876 eV	Electron donor power (ώ-)	4.0451 eV
Electron Affinity (EA)	0.4465 eV	Nucleofugality ΔEn	1.9002 eV
Absolute Hardness (η)	3.0700 eV	Electrofugality ΔEe	7.8413 eV
Absolute Softness (σ)	$0.3366eV^{-1}$	$\Delta E_{back\text{-}donation}$	-0.7426 eV

Drug likeness for C2D3O

A crucial first stage in the drug-development process, drug similarity aids researchers in locating possible lead compounds with advantageous pharmacokinetic and pharmacodynamic characteristics. In pharmacokinetics objects absorption, distribution, metabolism and excretion processes of drugs move through the body over time. It can be through the PKCSM analysis of this compound had descriptors with values in the (Table 4). Nevertheless, more experimental verification is required to evaluate the compound's true efficacy and safety. Rules and criteria have been devised to evaluate a compound's drug similarity.

One of the most often used criteria for determining whether a substance is likely to be orally active in humans is Lipinski's rule. This molecule conforms to the rule since it has two hydrogen bond acceptors, zero hydrogen bond donors, a molecular weight of 19.2 g/mol, a partition coefficient (logP) of less than 5, and a molecular weight of less than 500 g/mol[28]. According to Veber's Rules, the title compound's rotational bond is ≤ 10, which yields a value of 3. Polar surface area < 140 Å² restrictions also show that this compound has an achieved value of 86.071 Å². As an alternative, a molecule already meets the donors and acceptors of hydrogen bonds listed above. Additional parameters for drug similarity are provided by the Ghose filter. The number of atoms in this molecule is limited to 20–70, and the molecular weight between LogP and 34 is already satisfied.

Table 4 — C2D3O Parameters of Drug Likeness

Descriptor	Value
Molecular Weight	196.29 g/mol
LogP	2.751
Rotatable Bonds	3
Acceptors	2
Donors	0
Surface Area	86.071 Å²

MEP Analysis

This compound complies with the rule, as its molecular weight (196.29 g/mol) is below 500 g/mol, its logP (partition coefficient, indicating lipophilicity) is under 5, it has zero hydrogen bond donors, and it possesses two hydrogen bond acceptors[29].For medicinally significant compounds, the MEP diagram is well known for offering extremely helpful information for understanding or forecasting the chemical reactivity behavior of any molecular system[30].The highest negative electrostatic potential in (Fig. 4) is shown by red patches, which are electron-rich regions, mostly surrounding the oxygen atoms in the carbonyl (C=O) functional groups. Because of their high electron density, these sites are conducive to electrophilic assault. Blue patches, on the other hand, indicate the strongest electrostatic potential and are usually found near

hydrogen atoms that are joined to carbonyl groups or other areas that lack electrons, making them more vulnerable to nucleophilic assault. A balanced distribution of charges is indicated by green patches, which denote neutral electrostatic potential. Molecular docking studies and other molecular interactions can be greatly impacted by the existence of lone pairs on oxygen (LP (1) and LP (2) of O7 and O12), which indicate strong donor properties. A molecule's chemical reactivity and its uses in biological systems, especially in drug design where binding interactions are essential, are greatly influenced by the charge distribution seen in the MEP analysis. This technique is a useful tool for anticipating reactive sites and directing additional computational and experimental research.

Natural bond orbital (NBO) analysis

Using the natural bond orbital (NBO) analysis, the conjugative and hyper-conjugative interactions, intramolecular and intermolecular hydrogen bonds, and the electron density distribution between bonding and antibonding orbitals in the molecular system were identified[31]. For a select group of donors and acceptors, Table 5 displays the NBO computation along with the E (2), E(j)–E(i), and f (i, j) values.

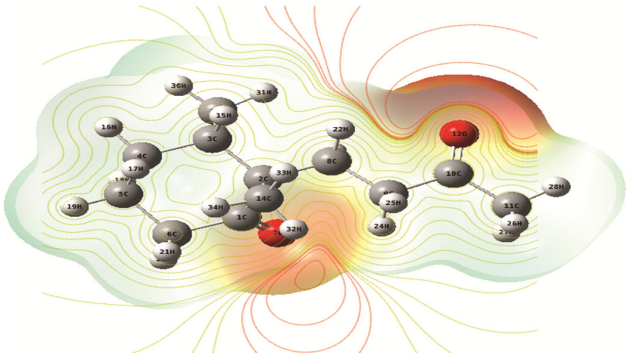

Fig. 4 — The MEP map surface on C2D3Ocompound

The stabilization energy E (2) of the NBO analysis is used to characterize the interaction between occupied and unoccupied NBO type Lewis's orbitals because they facilitate the electron delocalization from bonding (BD) or lone pair (LP) orbitals to anti-bonding (BD*) orbitals[32]. With O_7 LP (2) → C_1–C_6 σ∗ and O_{12} LP (2) →C_9–C_{10} σ∗ contributing 22.19 kcal/mol^{-1} and 20.72 kcal/mol^{-1}, respectively, the higher stabilization energies are found in the lone pair (LP) interactions of oxygen atoms (O7 and O12) with adjacent σ* orbitals. Strong electron delocalization is suggested by these interactions, which greatly stabilizes the molecule structure. The relevance of hyper conjugative interactions in molecule stability is further demonstrated by their noteworthy stabilization energies of 4.68 kcal/mol^{-1} for C_6 − H_{21} σ → C_1 − O_7 π∗ and 4.55 kcal/mol^{-1} for C_9 − H_{24} σ → C_{10} − O_{12} π∗. The observed hyperconjugation and charge delocalization support the molecule's overall electronic stability, which may affect its optoelectronic characteristics, chemical reactivity, and biological activity. The results obtained from this NBO analysis offer a better grasp of the electronic structure of the molecule and can be used as a starting point for additional experimental and computational research.

Topological analysis

A complete understanding of electron distribution and bonding is provided by the Electron Localization Function (ELF) and Localized Orbital Locator (LOL), which are frequently employed for surface and topological investigations of molecular systems. ELF τ(r) and LOL (r), which explain electron localization in terms of density and orbital interactions, are the

Table 5 — Second-order perturbation theory analysis of fock matrix in C2D3O

Donor(i)	Type	Acceptor(j)	Type	E (2) (Kcal/ mol^{-1})	E (j)-E (i) (a. u.)	F (i, j)(a. u.)
C_2 - C_3	σ	C_1 - O_7	π*	2.08	0.62	0.032
C_1 - C_6	σ	C_2 - C_8	σ*	1.93	1.04	0.040
C_6 -H_{21}	σ	C_1 - O_7	π*	4.68	0.53	0.045
C_8 - H_{23}	σ	C_9 - H_{25}	σ*	3.10	0.86	0.046
C_9 - H_{24}	σ	C_{10} - O_{12}	π*	4.55	0.53	0.044
C_9 - H_{25}	σ	C_{10} - O_{12}	π*	4.52	0.53	0.044
C_{11} -H_{26}	σ	C_{10} - O_{12}	σ*	4.69	1.13	0.065
C_{11} -H_{27}	σ	C_{10} - O_{12}	π*	4.64	0.53	0.045
C_{11} - H_{28}	σ	C_{10} - O_{12}	π*	4.62	0.53	0.045
O_7	LP (1)	C_1 - C_2	σ*	2.61	1.07	0.048
O_7	LP (2)	C_1 - C_2	σ*	21.27	0.66	0.107
O_7	LP (2)	C_1 - C_6	σ*	22.19	0.65	0.109
O_{12}	LP (2)	C_9 - C_{10}	σ*	20.72	0.67	0.107
O_{12}	LP (2)	C_{10} - C_{11}	σ*	20.88	0.65	0.106

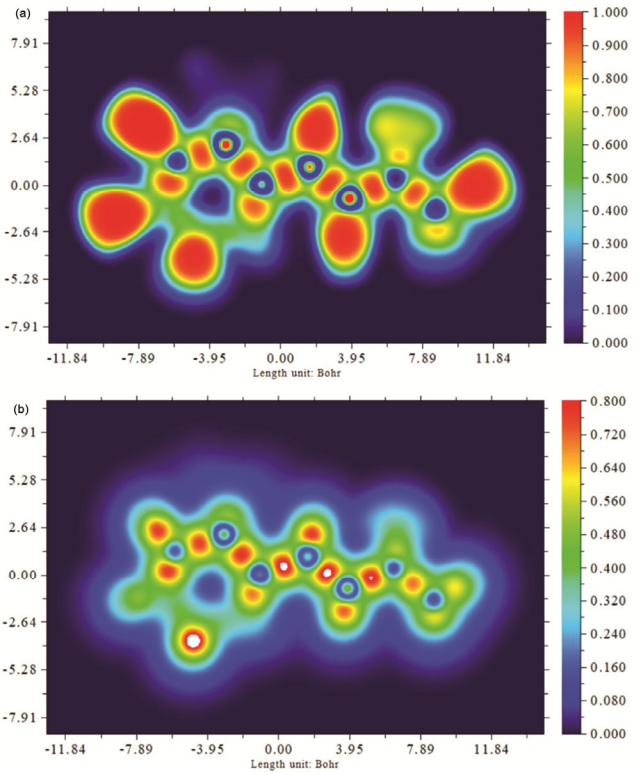

Fig 5 — (a) ELF map of C2D3O; and (b) LOL map of C2D3O

foundation of these techniques, which help interpret covalent bonds and electronic structures [33, 34]. Using Multiwfn 3.7 software, ELF and LOL analyses were performed on the title chemical in this study. The results are displayed in Figure 5a and b as color field projection maps and contour maps. The blue-to-red color gradient represents the ELF values, which range from 0.0 to 1.0. Aside from the regions that surround atomic nuclei, red areas denote regions with high electron localization, like lone pairs, whereas blue regions that join atoms show lesser electron localization, which is typical of covalent bonds. This is enhanced by the LOL analysis, which offers further information for values between -11.84 and 11.84 Bohr. Electron localization is shown by the matching colour scale, which ranges from blue to red 0.0 to 0.80[35, 36]. Whereas blue regions, which frequently have wider contour spacing, indicate areas of poorer electron localization, red portions in LOL maps indicate electron-rich places, such as lone pairs and bonding regions. In addition to disclosing the molecule's electrical structure, these investigations offer important insights into the system's atomic connections and biological interactions. Combining ELF and LOL research improves knowledge of bonding properties and electron density distribution, which makes it a crucial method for molecular research.

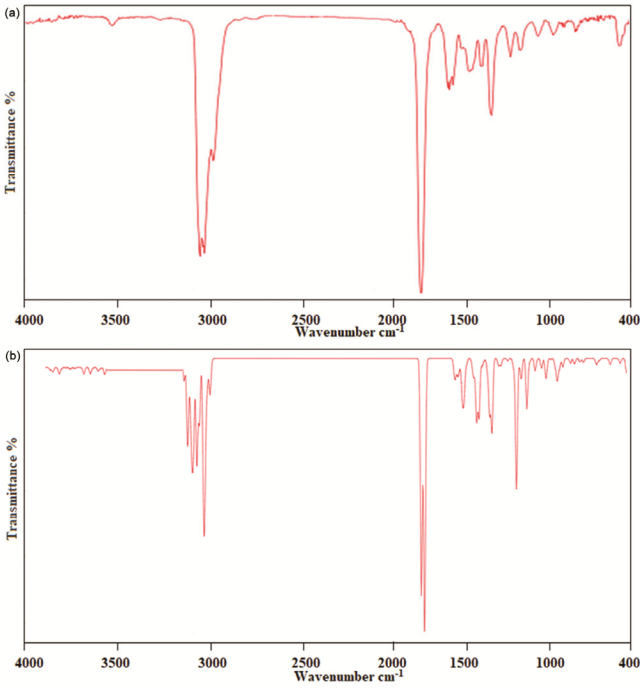

Fig 6 — FT-IR of C2D3O

FT-IR of C2D3O

Vibrational analysis of C2D3O was to be used to identify different types of vibrations inside the molecule. The vibrational frequencies for two distinct basis sets, 6-31G (d, p) and 6-311++G (d, p), were computed using the B3LYP technique[37]. The VEDA 4 software was used to calculate the PED, which determines the relative contributions of various molecular components to each vibration. Table 6 displays the findings of these investigations. After deducting the three translational and three rotational degrees of freedom, the formula 3N-6 provides the total number of possibly visible vibrational modes for a nonlinear molecule with N atoms[38]. Since the molecular structure of C2D3O is symmetric in the C1 point group, it is not possible to considerably simplify the vibrational modes based on symmetry. All vibrations are active in both the Raman and infrared (IR) spectra. The force constants derived from the vibrational analysis were used to calculate the PED, which allowed each vibrational mode to be linked to distinct molecular movements. This is because the 34 atoms in C2D3O are expected to exhibit 96 typical vibrational modes. Figure 6 shows a high correlation between the measured C2D3O FT-IR spectra and the calculated vibrational frequencies. For the vibrational study of MMDT, several vibrational modes—including C=C, C–C, CH_3, CH_2, CO, C–H,

Table 6 — FT-IR of C2D3O

B3LYP/6-311++G (d.p)	Experimental	Vibrational Assignment +PED		B3LY P/6-311++G (d.p)	Experimental	Vibrational Assignment +PED	
3162		υCH	70	1159	1151	δHCC	15
3144	3144	υCH	71	1112	1100	υCC	11
3139		υCH	77	1070	1180	υCC	36
3126		υCH	65	1019		υCC	11
3118		υCH	95	994	1000	υCC	28
3117		υCH	79	968		υCC+τHCCC	16+14
3110		υCH	46	957		τHCCC	15
3108		υCH	45	925		δHCC	14
3091	3098	υCH	65	859	850	δHCC+ τHCCC	10+10
3077	3070	υCH	39	810		υCC	16
3056	3061	υCH	65	736		τHCCC	12+10
3053		υCH	21	720		τHCCC+γOCCC	12+21
3050	3049	υCH	50	604		υCC	25
3046		υCH	85	568	550	δOCC	26
3045		υCH	57	531	530	δCCC	16
3044	3038	υCH	70	494		δCCC	11
3031		υCH	92	477		τHCCC+γOCCC	16+52
3016	3000	υCH	91	477		γOCCC	52
1810		υOC	90	442	420	δCCC	10
1792		υOC	91	412		δCCC+ τCCCC	26+10
1535	1540	δHCH	55	401	401	δCCC	12
1529	1528	δHCH	29	333		δCCC	19
1521		δHCH	20	318		υCC+δCCC	10+34
1514	1514	δHCH	30	283		δCCC	11
1509	1503	δHCH	38	283		τCCCC	10
1501	1500	δHCH	56	271		δCCC	13
1491	1495	δHCH+τ HCCC	47	271		τHCCC	32
1488		δHCH	65	244		δCCC	14
1483		δHCH	74	244		τHCCC	10
1479		δHCH+τHCCC	32	244		τHCCC	13
1466	1463	δHCH	69	221		δCCC	14
1432	1440	δHCH	47	221		δCCC	15
1425		δHCH	55	215		υCC	11
1410	1412	τHCCC+δHCH	32	215		δCCC	14
1396		δHCH	10	215		τHCCC	16
1394		δHCC+ γCCCH + τHCCC	29	196		δCCC	17
1379	1380	γCCCH	14	150		δHCH	20
1369		τHCCC	32	144		τHCCC	11
1350	1350	δHCC	12	134		δHCC	15
1346		δHCC+ τHCCC	26	123		δHCC	21
1336		δHCC	31	108		δCCC	34
1323		δHCC+τHCCC	32	108		τHCCC	10
1286	1280	δHCC	24	97		τHCCC	36
1273		δHCC	23	64		δCCC	33
1196		τCCCC	10	13		δHCC	50
1186		δOCC+STRECC	13 + 14				

HCC, HCCC, CCCH, and HCH—were mapped in order to examine their contributions to molecular dynamics. According to FTIR spectroscopy, a molecule's single bond status (saturated) or double or triple bond status (unsaturated) is described by its saturation and unsaturation. These structural features affect the apparent absorption peaks in the FTIR spectrum.

CH Vibrations

Typically, C-H stretching vibrational bands are seen in the 3100–3000 cm^{-1} range[39]. In the experimental FT-IR spectrum, the CH stretching vibrations in the investigated molecule are detected at 3144 cm^{-1}, 3098 cm^{-1}, 3070 cm^{-1}, 3061 cm^{-1}, 3049 cm^{-1}, 3038 cm^{-1}, and 3000 cm^{-1}. Density Functional Theory (DFT) with the B3LYP/6-311++G (d, p) basis set

yielded the following related computational values: 30144 cm^{-1}, 3091 cm^{-1}, 3077 cm^{-1}, 3056 cm^{-1}, 3050 cm^{-1}, 3044 cm^{-1}, and 3016 cm^{-1}. The theoretical approach correctly depicts the vibrational properties of the CH groups, as evidenced by the strong agreement between the experimental and computational values, respectively. These modes' relative contributions from the Potential Energy Distribution (PED) study are 71%, 65%, 39%, 65%, 50%, 70%, 55%, and 29%, indicating that they are primarily CH stretching vibrations with little to no mixing with other modes. The reliability of the computational technique in analysing the vibrational characteristics of the CH bonds in the molecule is demonstrated by this alignment of experimental and computational data.

HCCC, HCC Vibration

The C-H bond's bending modes in HCCC torsion and HCC scissoring mode in-plane bending are frequently located in the range of 1460–1480 cm^{-1} and 600–900 cm^{-1} [40]. The calculated HCCC, HCC values of 1535 cm^{-1}, 1526 cm^{-1}, 1514 cm^{-1}, 1509 cm^{-1}, 1501 cm^{-1}, 1491 cm^{-1}, 1466 cm^{-1}, 1432 cm^{-1}, 1410 cm^{-1}, 1379 cm^{-1}, 1350 cm^{-1}, 1286 cm^{-1}, 1159 cm^{-1}, 1259 cm^{-1}, and 841 cm^{-1} are correlated with the experimental values of 1540 cm^{-1}, 1503 cm^{-1}, 1500 cm^{-1}, 1495 cm^{-1}, 1463 cm^{-1}, 1440 cm^{-1}, 1412 cm^{-1}, 1380 cm^{-1} has an out of plane bending at this range CCCH , 1350 cm^{-1}, 1280 cm^{-1} and 1151 cm^{-1} to get the PED values of 55%, 29%, 30%, 38%, 56%, 47%, 69%, 47%, 39%, 14%, 12%, 24% and 15%.

CC, OCC, CCCC Vibration

In aromatic compounds, C = C and C - C, CCCC, OCC stretching vibrations usually show bands between around 500 and 700 cm^{-1} [41]. The computational values derived using the B3LYP/6-311++G (d, p) approach and the experimental FT-IR data for the C–C and C=C vibrational modes are found to be in good agreement. A trustworthy forecast is shown by the C–O stretching vibration, which has a computational value of 1792 cm^{-1}, 1810 cm^{-1}. Likewise, the observed FTIR result of 1240 cm^{-1} is consistent with the C=C stretching vibration, which is computed at 1242 cm^{-1}.Since these vibrational modes fall within the anticipated range for C–C and C=C stretching frequencies, it can be demonstrated that there is a strong correlation between the computational predictions and the experimental evidence. The B3LYP/6-311++G (d, p) method's accuracy in predicting vibrational properties is confirmed by this alignment between theory and experiment, which meets the predicted values for these functional groups. Wave counts of 994 cm^{-1}, 859 cm^{-1}, 568 cm^{-1}, and 531 cm^{-1} have been reported. These match the PED values of 28%, 26%, 16%, 10%, and 12% for the experimental wave numbers of 1000 cm^{-1}, 850 cm^{-1}, 550 cm^{-1}, and 530 cm^{-1}.

C2D3O of UV-Vis

The UV spectrum in the gas phase is shown in (Fig. 7), while Table 6 displays the molecule's predicted wavelength, energy, bond gap, and oscillator strength. The n-p transition is less evident than the p-p transition[42]. The n or p orbitals transition to an excited state using the absorbance spectroscopy technique. In addition, we reported the energy of the orbitals and computed the energy gap between the principal peaks of the molecular orbitals of the spectra and the border HOMO–LUMO orbitals[43]. The electron transition at 287.53 nm, excitation energy = 4.3121 eV, and oscillation strength f = 00.0001 in the current study closely resembles the experimental UV-visible spectra absorption at 269 nm, which represents the $\pi \rightarrow \pi^*$ electronic transition from ground state to excited state in the C2D3O compound. Quantum chemistry theory was used to analyze the electronic transition features of C2D3O utilizing the UV-visible spectra and related properties of oscillation strengths (f), excitation energy (eV), and absorption band (nm). These features are based on the DFT/B3LYP/6-311++G(d, p) method, which was computed in the gas phase and connected to real UV-visible spectra. Nevertheless, further absorption transitions at 289.12 and 226.78 nm, respectively, are

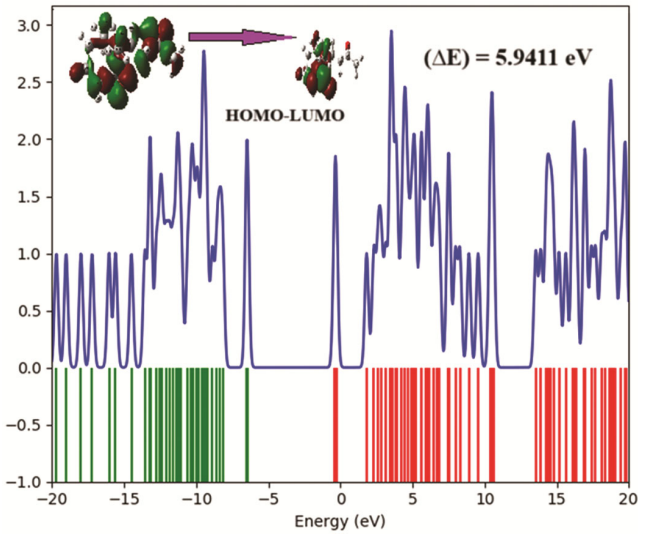

Fig. 7 — Uv-Vis of C2D3O

not consistent with the experimental values listed in (Table 7). The Gauss Sum software found that the largest contributions were HOMO->L+1 (94%), H-1->LUMO (94%), and HOMO->LUMO (94%), whereas the smallest contributions were HOMO->LUMO (4%), H-1->L+1 (3%), and HOMO->L+1 (4%). The Gauss Sum software found that the largest contributions were HOMO->L+1 (94%), H-1->LUMO (94%), and HOMO->LUMO (94%), whereas the smallest contributions were HOMO->LUMO (4%), H-1->L+1 (3%), and HOMO->L+1 (4%).

C2D3O of DOS

The density of states (DOS) is an important word in electronic structure study since it gives information on how electronic states are distributed across energy levels in material[44]. Knowing how various atoms and orbitals contribute to the electronic structure is necessary to comprehend the material's features, including conductivity, optical behaviour, and bonding properties of the C2D3O. It explains how the distribution pattern around HOMO and LUMO is influenced by the type of acceptor moieties that remove electrons. For DOS interpretation, each structure is separated into donor and acceptor portions[45]. As can be seen in Figure 8, the donor's relative intensity is displayed in green, and the acceptors' relative intensity is displayed in red. On DOS graphs, HOMO is represented by negative values along the x-axis, whereas LUMO is represented by positive numbers.

Table 7 — UV-Vis of C2D3O

		B3LYP/6-311G(d,p)				
Solvents	States	Absorption b and λ (nm)	Excitation energies (cm^{-1})	Oscillation Strength f	Energy Gap (eV)	Major Contributions Energy (%)
Gas Phase	S1	289.12	34588.28	0.0001	402884	HOMO->L+1 (94%) HOMO->LUMO (4%)
	S2	287.53	34779.43	0.0000	4.3121	H-1->LUMO (94%) H-1->L+1 (3%)
	S3	226.78	44095.94	0.0000	5.4672	HOMO-> LUMO (94%) HOMO-> L+1 (4%)
Experimental		287	-	-	-	-

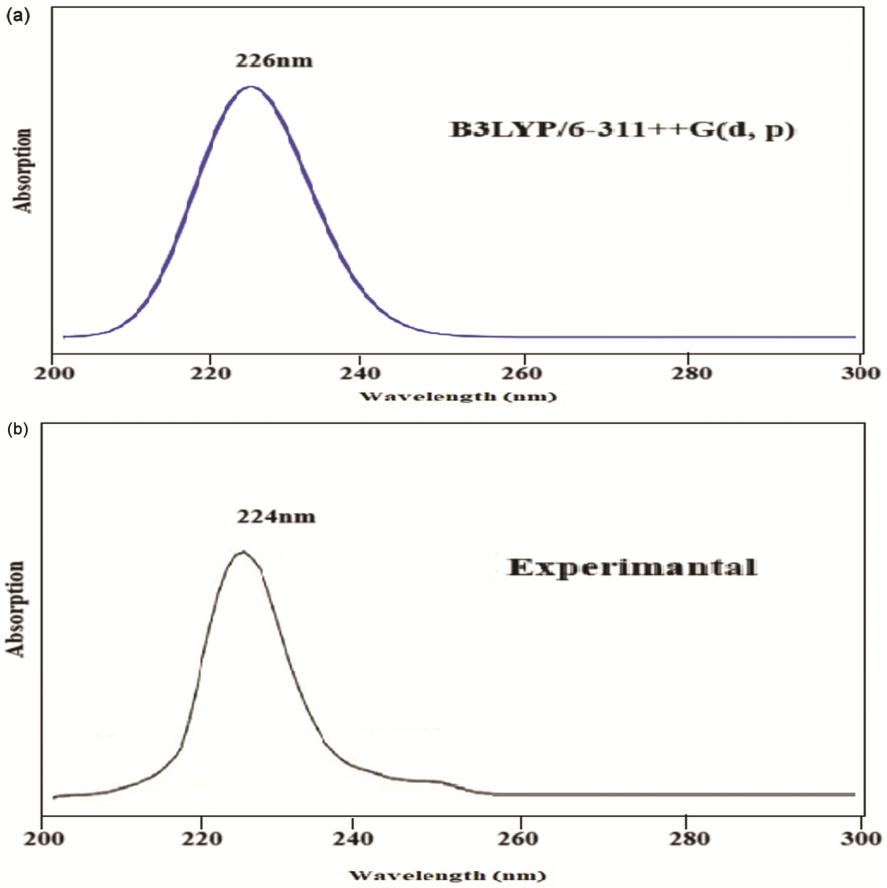

Fig. 8 — C2D3O of DOS

Table 8 — Molecular Docking of C2D3O

Protein (PDB ID)	No. of hydrogen bond	Bond distance (Å)	Bonded residues	Estimated Inhibition Constant (μm)	Binding energy (kcal/mol)	Reference RMSD (Å)
8D59	2	2.2	ARG`124 (O... 2HH1)	237.85	-4.94	4.81
		1.9	ARG`121 (O… 1HH2)			

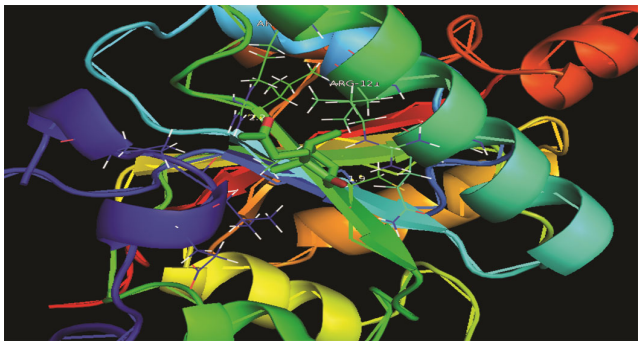

Fig. 9 — Molecular docking of C2D3O

The donor groups in the molecule C2D3O have a somewhat larger concentration of the HOMO's electron density, which is dispersed across the molecule[46]. Although some electron density is linked to the donor groups, the acceptor moiety is the main source of electron density in the LUMO. The acceptor group in the LUMO has a higher electron density than the donor group. These results show that the withdrawing activity of the end-capped acceptor moieties is sufficient.

Molecular Docking

A structure-based method for designing drugs, molecular docking models receptor-ligand interactions to forecast binding affinities and modalities. Examining biomolecular interactions and supporting logical drug design, makes drug discovery easier. This approach is a useful research tool since it calculates binding energy, free energy, and complex stability. The PDB structures of target proteins were obtained from the RCSB protein data library[47-49]. The downloaded inhibitor protein, identified as 8D59, was selected for docking with the sample compound. AutoDock was used for molecular docking, where the ligand and water molecules were separated from the protein. Additionally, polar hydrogen bonds and Geisteger charges were introduced during the process. Docking parameters, including RMSD value, hydrogen bond count, bond distances, bonded residues, inhibition constant, and binding energy, are summarized in (Table 8 & Fig. 9).

The 8D59 protein inhibitor exhibited a low binding energy of -4.94 kcal/mol and a high RMSD value of 43.81, indicating interaction stability. In docking studies, binding energy represents the energy released upon ligand-protein interaction, with higher binding energy signifying a stronger bond. The results illustrate that a hydrogen bond is formed between the hydrogen atom of the ligand and the carbon atom of the protein inhibitor[50]. Generally, hydrogen bonds occur when hydrogen is covalently attached to an electronegative atom (such as nitrogen or oxygen) and interacts with another atom possessing a lone pair of electrons. The ligand exhibits a high binding affinity for the target protein, demonstrating structural similarity between the ligand and the inhibitor protein.

Conclusion

Using the gas chromatography-mass spectrometry (GC–MS) approach, the C2D3O molecule is being conformed in *Hybanthus enneaspermus* crude. Optimized structural conformation and electronic characteristics were investigated using the B3LYP method, the 6-311++G (d, p) basis set, and experimental techniques such as UV-Vis and FT-IR. Each atom's vibrational statement may be examined in the analyses. O7 LP (2) → C1−C6 σ∗ and O12 LP (2) →C9−C10 σ∗ contribute 22.19 kcal/mol^{-1} and 20.72 kcal/mol^{-1} to the C2D3O, respectively, according to NBO. Topological research like ELF and LOL have values between 0.0 and 1.0 and blue to red between 0.0 and 0.80. The present analysis of the UV-visible spectra shows an electron transition at 287.53 nm, an excitation energy of 4.3121 eV, and an oscillation strength of f = 00.0001. The density of states (DOS) of material also shows the distribution of electronic states across energy levels, with HOMO->L+1 (94%), H-1->LUMO (94%), and HOMO->LUMO (94%). With an estimated inhibition constant binding distance of 237.85 μm and 2.2 ARG~124, 1.9 ARG`121 residues, the ligand exhibits a high binding affinity for the target protein of -4.94 kcal/mol.

Conflict of interest

All authors declare no conflict of interest.

References

1 Sapnakumari M, Divya K, Aswin KB & Dalin J, Antimicrobial and Antioxidant Study of Some Newly Synthesized Chalcones and Cyclohexenone Derivatives. *Asian J Chem*, 35 (2023).

2 Rahim NFC, Hussin Y, Aziz MNM, Mohamad NE, Yeap SK, Masarudin MJ, Abdullah R, Akhtar MN & Alitheen NB, Cytotoxicity and apoptosis effects of curcumin analog (2E, 6E)-2, 6-Bis(2, 3-Dimethoxybenzylidine) cyclohexanone (DMCH) on human colon cancer cells HT29 and SW620 *in vitro*. *Molecules*, 26 5(2021) 1261.

3 Revalde JL, Li Y, Hawkins BC, Rosengren RJ & Paxton JW, Heterocyclic cyclohexanone monocarbonylanalogs of curcumin can inhibit the activity of ATP-binding cassette transporters in cancer multidrug resistance. *Biochem Pharmacol*, 93 (2015) 3, 305.

4 Prabhu C, Rajesh P, Vijayalakshmi D, Parthasarathy M, Dhanalakshmi E & Gowthami V, Kinetic Stability and Spectroscope investigation of Octadecanoic Acid- 17-Oxo-MethylEster (OA17OME). *Neuro Quantology*, 20 (2022) 2098.

5 Sevvanthi S, Muthu S, Aayisha S, Ramesh P & Raja M, Spectroscopic (FT-IR, FT-Raman and UV-Vis), computational (ELF, LOL, NBO, HOMO-LUMO, Fukui, MEP) studies and molecular docking on benzodiazepine derivatives- heterocyclic organic arenes. *Chem Data Collect*, 30 (2020) 100574.

6 Gomes AR, Varela CL, Tavares-da-Silva EJ & Roleira FMF, Epoxide containing molecules: A good or a bad drug design approach. *Eur J Med Chem*, 201 (2020) 112327.

7 Patel DK, Krishnamurthy S & Hemalatha S, Evaluation of glucose utilization capacity of bioactivity guided fractions of *Hybanthus enneaspermus* and Pedalium murex in isolated rat hemidiaphragm. *J Acute Dis*, 2 (2013) 33.

8 Narayanswamy VB, Manjunatha Setty M, Malini S & Shirwaikar A, preliminary aphrodisiac activity of *Hybanthus enneaspermus* in rats. *Pharmacologyonline*, 1 (2007) 152.

9 Rajesh P, Kandan P, Sathish S, Manikandan A, Gunasekaran S, Gnanasambandan T & Abiramig Sb, Vibrational spectroscopic, UV-Vis, molecular structure and NBO analysis of Rabeprazole. *J Mol Struct*, 1137 (2017) 277.

10 Mohammed K, Mohammed AAK, Abdel Hakiem AFA & Mahfouz RM, Computational evaluation on the molecular conformation, vibrational spectroscopy, NBO analysis and molecular docking of betaxolol and betaxolol-chlorthalidone cocrystals. *J Mol Struct*, 1209 (2020) 127744.

11 Thendral ED, Gomathi S, Sumaya UM, Biruntha K & Usha G, 1-(Pyridin-2-yl)-2, 4-bis [(pyridin-2-yl)carbonyl]-3, 5-bis(3, 4, 5-trimethoxyphenyl)cyclohexanol 2.25-hydrate. *Acta Cryst*, 2 (2017) 2414.

12 Govindaraju M, Vennila P, Venkatesh G, Kamal C, Mary YS, Panicker CY, Kaya S, Armakovic S & Armakovic SJ, A complete computational and spectroscopic study of 2-bromo-1, 4-dichlorobenzene - a frequently used benzene derivative. *J Mol Struct*, 1151 (2018) 245.

13 Chandralekha K, Gavaskar D, Sureshbabuc AR & Lakshmia S, 5′-Benzyl--idene-1″ -methyl-4″- phenyl -tri- spiro- [1, 3-dioxolane-2, 1′-cyclo-hexane-3′, 3″-pyrrolidine-2″, 3‴-indole] -4′, 2‴-dione. *Acta Crystallogr*, 2 (2017) 5.

14 Samshuddin S, Jasinski JP, Butcher RJ, Neuhardt EA, Narayana B & Yathirajan HS & Glidewell C, Three closely-related cyclohexanols (C35H27X2N3O3; X = F, Cl or Br): similar molecular structures but different crystal structures, *Acta Cryst*, (2014) 953.

15 Jebapriya JC, Jonathan DR, Prasanaa JC & Usha G, (2E)-2-[4-(Di-methyl-amino)-benzyl--idene]-5-methyl-cyclo-hexa-none. *Acta Crystallogr*, 2 (2017).

16 Shirmila DA, Jonathan DR, Priya MK, Hemalatha J & Usha G, (2E)-2-(3, 4-Di-methoxy-benzyl--idene)-3, 4-di-hydro-naphthalen-1(2H)-one. *Acta Crystallogr*, 6 (2021).

17 Zhang LJ, Koua JF & Liua FY, 4-(2, 4, 6-Trimethylphenyl) butan-2-one. *Acta Crystallogr*, 2 (2017).

18 Chen H & Sun J, Selective hydrogenation of phenol for cyclohexanone: A review. Korean Society of Industrial Engineering Chemistry. *J Ind Eng Chem*, 94 (2021) 78.

19 Jia S, Tan X, Wu L, Ma X, Zhang L, Feng J, Xu L, Song X, Zhu Q, Kang X, Sun X & Han B, Integration of plasma and electrocatalysis to synthesize cyclohexanone oxime under ambient conditions using air as a nitrogen source. *Chem Sci*, 14 (2023) 13198.

20 Hollebeek T, Ho T-S & Rabitz H, Constructing multidimensional molecular potential energy surfaces from ab initio data. *Annu Rev Phys Chem*, 50 (1999) 537.

21 Sevvanthi S, Muthu S, Raja M, Aayisha S & Janani S, PES, molecular structure, spectroscopic (FT-IR, FT-Raman), electronic (UV-Vis, HOMO-LUMO), quantum chemical and biological (docking) studies on a potent membrane permeable inhibitor: dibenzoxepine derivative. *Heliyon*, 6 (2020) 8.

22 Prabhaharan M, Prabakaran AR, Srinivasan S & Gunasekaran S, Density functional theory studies on molecular structure, vibrational spectra and electronic properties of cyanuric acid. *Spectrochim*, 138 (2015) 711.

23 Ceylan U, Çapan A, Yalçın ŞP, Sönmez M & Aygün M, Vibrational spectroscopic and thermo dynamical property studies, Fukui functions, HOMO-LUMO, NLO, NBO and crystal structure analysis of a new Schiff base bearing phenoxy-iminegroup. *J Mol Struct*, 1136 (2017) 222.

24 Abdullah MN, Osw P, Hassan SA & Othm S, two new cyclohexenone derivatives: Synthesis, DFT estimation, biological activities and molecular docking study. *J Mol Struct*, 1301 (2024) 222.

25 Uddin N, Rashid F, Haider A, Tirmizi SA, Raheel A, Imran M, Zaib S, Diaconescu PL, Iqbal J & Ali S, Triorganotin (IV) carboxylates as potential anticancer agents: Their synthesis, physiochemical characterization, and cytotoxic activity against HeLa and MCF-7cancer cells. *Appl Organomet Chem*, 35 (2021) 4.

26 Antony I, John D, Jebaraj W, Kores JJ & Sasitha T, DFT, NBO, HOMO-LUMO, NCI, stability, Fukui function and hole – Electron analyses of tolcapone. *Comput Theor Chem*, 1202 (2021) 113296.

27 Rahumana MH, Muthua S, Raajaramanc BR, Rajad M & Umamahesvarie H, Investigations on 2-(4-Cyanophenylamino) acetic acid by FT-IR, FT-Raman, NMR and spectroscopy, DFT (NBO, HOMO-LUMO, MEP and Fukui function) and molecular docking studies. *Heliyon*, 6 (2020) 9.

28 Daina A, Michielin O & Zoete V, Swiss ADME: A free web tool to evaluate pharmacokinetics, drug-likeness and medicinal chemistry friendliness of small molecules. *Sci Rep*, 7 (2017) 42717.

29 Laura JJ, Rajesh P, Kesavan M, Dhanalakshmi E, Kayashrini S & Prabhaharan M, Degree–based topological indices, NMR chemical shifts, chemical reactivity, molecular dynamics and DFT analysis of 1, 4-Methanoazulene-9-methanol, Decahydro-4, 8, 8-trimethyl-,[1S-(1α, 3aβ, 4α, 8aβ, 9R)]. *Biophys Chem*, 322 (2025) 107442.

30 Uluda N & Serdaroglu G, An improved synthesis, spectroscopic (FT-IR, NMR) study and DFT computational

analysis (IR, NMR, UVe Vis, MEP diagrams, NBO, NLO, FMO) of the 1, 5-methanoazocino[4, 3-b] indole core structure. *J Mol Struct*, 1155 (2018) 548.

31 Abedin MM, Alam MA, Pal TK & Sheikh MC, Investigation on synthesized sulfonamide Schiff base with DFT approaches and *in silico* pharmacokinetic studies: Topological, NBO, and NLO analyses. *Heliyon*, 10 (2024) 14.

32 Vasanthi T, Balasubramanian V & Vijayakumar VN, Theoretical studies (DFT) on hydrogen bonded liquid crystal derived from 4-amino and 4-dodecyloxy benzoic acids. *Mater Today Proc*, 47 (2021) 1724.

33 Laura JJ, Rajesh P, Kayashrini S & Abirami SB, Kojibiose as a Sustainable Bioactive Molecule: Experimental and DFT Insights into Antibacterial Activity and Electronic Properties. *J Mol Struct*, (2026) 145576.

34 Kayashrini S, Rajesh P, Dhanalakshmi E, Kesavan M, Prabhaharan M, Al Farraj DA & Elshikh MS, FT-IR, UV–Vis, density functional theory and molecular docking studies on 3, 7, 11, 15-Tetramethyl-2hexadecen-1-ol. *J Mol Struct*, 1321 (2025) 139600.

35 Manjusha P, Prasanna JC, Muthu S & Rizwana BF, Spectroscopic elucidation (FT-IR, FT-Raman and UV-visible) with NBO, NLO, ELF, LOL, drug likeness and molecular docking analysis on 1-(2-ethylsulfonylethyl)-2-methyl-5-nitro-imidazole: an antiprotozoal agent. *Comput Biol Chem*, 88 (2020) 107330.

36 Subbaiah S, Elangovan N, Ajithkumar G & Manoj KP, (E)-4-((4-Bromobenzylidene) Amino)-N-(Pyrimidin-2-yl) Benzenesulfonamide from 4-Bromobenzaldehyde and Sulfadiazine, Synthesis, Spectral (FTIR, UV–Vis), Computational (DFT, HOMO–LUMO, MEP, NBO, NPA, ELF, LOL, RDG) and Molecular Docking Studies. *Polycycl Aromat Com*, 42 (2022) 10.

37 Vincy CD, Tarika JDD, Dexlin XDD, Rathika A & Beaula JT, Exploring the antibacterial activity of 1, 2 diaminoethane hexanedionic acid by spectroscopic, electronic, ELF, LOL, RDG analysis and molecular docking studies using DFT method. *J Mol Struct*, 1247 (2022) 131388.

38 Rajesh P, Gunasekaran S, Gnanasambandan T & Seshadri S, Experimental, quantum chemical and NBO/NLMO investigations of pantoprazole. *Acta*, 136 (2015) 247.

39 Arumugam T, Ramalingam A, Guerroudj AR, Sambandam S, Boukabcha N & Chouaih A, Conformation and vibrational spectroscopic analysis of 2, 6-bis (4-fluorophenyl)-3, 3-dimethylpiperidin-4-one (BFDP) by DFT method: A potent anti-Parkinson's, anti-lung cancer, and anti-human infectious agent. *Heliyon*, 10 (2024) 30.

40 Kumari RV, Nirmala W, Sagadevan CS, Mugeshini S, Rajeswari N, Balue R & Kumari RS, Synthesis, growth, crystal structure, vibrational, DFT and HOMO, LUMO analysis on protonated molecule-4-aminopyridinium nicotinate. *J Mol Struct*, 239 (2021) 130449.

41 Rocha M, Santo AD, Arias JM, Gil MD & Altabef AB, Ab-initio and DFT calculations on molecular structure, NBO, HOMO-LUMO study and a new vibrational analysis of 4-(dimethylamino) benzaldehyde. *Acta A Mol Biomol Spectrosc*, 136 (2015) 130449.

42 Kayashrini S, Rajesh P, Kesavan M, Kala A & Pavithra M, Application of Degree-Based Topological Descriptors, Molecular Properties, Chemical Reactivity Prediction and Nonlinear Optical Analysis of 5- [2- [4-(1, 2-benzothiazol-3-yl) piperazin-1-yl] ethyl]-6-chloro-1, 3-dihydroindol-2-one. *J Mol Struct*, 1354 (2025) 144847.

43 Khemalapure SS, Katti VS, Hiremath CS, Hiremath SM, Basanagouda M, Shivaraj B Radder SB, Spectroscopic (FT-IR, FT-Raman, NMR and UV-Vis), ELF, LOL, NBO, and Fukui function investigations on (5-bromo-benzofuran-3-yl)-acetic acid hydrazide (5BBAH): Experimental and theoretical approach. *J Mol Struct*, 1196 (2019) 280.

44 Dhanalakshmi E, Rajesh P,Arunkumar K, Gnanasambandan T, Noureddine ISSAOUI, Sudha K & Raja M, Synthesis, GCMS, spectroscopic, electronic properties, chemical reactivity, RDG, topology and biological assessment of 1-(3,6,6-trimethyl-1,6,7,7a-tetrahydrocyclopenta[c]pyran-yl) ethenone. *Chem Phys Impact*, 7 (2023) 100385.

45 Mekoung PMA, Malloum A, Govindarajan M, Mballa RN, Patouossa I, Zintchem AAA, Nanseu CPN & Mbouombouo IN, Spectroscopic properties (FT-IR, NMR and UV) and DFT studies of amodiaquine. *Heliyon,* 9 (2023) 12.

46 Shafiq I, Khalid M, Jawaria R, Shafiq Z, Murtaza S & Braga AAC, Exploring the photovoltaic properties of naphthalene-1,5-diamine-based functionalized materials in aprotic polar medium: a combined experimental and DFT approach. RSC Advances, 45 (2024)33048–33060.

47 Fan J, Fu A & Zhang L, Progress in molecular docking. *Quant Biol*, 7 (2019) 83.

48 Dexlin XDD, Tarika JDD, Kumar SM, Mariappan A & Beaula TJ, Synthesis and DFT computations on structural, electronic and vibrational spectra, RDG analysis and molecular docking of novel Anti COVID-19 molecule 3, 5Dimethyl Pyrazolium 3, 5 Dichloro Salicylate. *J Mol Struct*, 1246 (2021) 131165.

49 Maiolo FD & Painelli A, Intermolecular energy transfer in real time. *J Chem Theor Comput*, 14 (2018) 5339.

50 Zha GF, Qin HL, Youssif BGM, Amjad MW, Raja MAG, Abdelazeem AH & Bukhari SNA, Discovery of potential anticancer multi-targeted ligustrazine based cyclohexanone and oxime analogy overcoming the cancer multidrug resistance. *J Med Chem*, 135 (2017) 34.